Journal of Experimental Botany Advance Access published September 9, 2015

Journal of Experimental Botany
doi:10.1093/jxb/erv416

REVIEW PAPER

Solid-state NMR investigations of cellulose structure and interactions with matrix polysaccharides in plant primary cell walls

Tuo Wang and Mei Hong*

Department of Chemistry, Massachusetts Institute of Technology, 170 Albany Street, Cambridge, MA 02139, USA

* To whom correspondence should be addressed. E-mail: meihong@mit.edu

Received 15 May 2015; Revised 30 July 2015; Accepted 11 August 2015

Editor: Simon Turner

Abstract

Until recently, the 3D architecture of plant cell walls was poorly understood due to the lack of high-resolution techniques for characterizing the molecular structure, dynamics, and intermolecular interactions of the wall polysaccharides in these insoluble biomolecular mixtures. We introduced multidimensional solid-state NMR (SSNMR) spectroscopy, coupled with ^{13}C labelling of whole plants, to determine the spatial arrangements of macromolecules in near-native plant cell walls. Here we review key evidence from 2D and 3D correlation NMR spectra that show relatively few cellulose–hemicellulose cross peaks but many cellulose–pectin cross peaks, indicating that cellulose microfibrils are not extensively coated by hemicellulose and all three major polysaccharides exist in a single network rather than two separate networks as previously proposed. The number of glucan chains in the primary-wall cellulose microfibrils has been under active debate recently. We show detailed analysis of quantitative ^{13}C SSNMR spectra of cellulose in various wild-type (WT) and mutant *Arabidopsis* and *Brachypodium* primary cell walls, which consistently indicate that primary-wall cellulose microfibrils contain at least 24 glucan chains.

Key words: *Arabidopsis*, *Brachypodium*, cellulose microfibrils, dynamics, intermolecular contact, multidimensional correlation NMR.

Introduction

Plant primary cell walls contain many macromolecules, including cellulose, hemicelluloses, pectins, and glycoproteins. Cellulose microfibrils consist of linear glucan chains that are held together by hydrogen bonds and other non-covalent interactions (Nishiyama *et al.*, 2002, 2003b; Jarvis, 2003). In dicotyledonous plants, the main hemicellulose is xyloglucan (XyG), which are glucan chains substituted with Xyl, Gal, and Fuc sidechains (Fry, 1989; Park and Cosgrove, 2015). In grass primary walls, the main hemicelluloses are glucuronoarabinoxylan (GAX) and mixed-linkage glucan (MLG). GAX has a β-(1,4)-linked xylose (Xyl) backbone and Ara and glucuronic acid (GlcA) sidechains, while MLGs are unbranched chains of ~30% β-(1,3) and ~70% β-(1,4)-linked glucopyranosyl residues (Woodward *et al.*, 1988; Kiemle *et al.*, 2014). Pectins are acidic polysaccharides rich in galacturonic acid (GalA) residues. In dicot primary cell walls, both linear homogalacturonan (HG) and branched rhamnogalacturonan (RG) with arabinose and galactose (Gal) sidechains are present (Caffall and Mohnen, 2009), while grass primary walls contain only low concentrations of pectins (Vogel, 2008).

Abbreviations: b, surface-bound interior cellulose; c, core interior cellulose; DQF, double-quantum-filtered; G, glucose in xyloglucan; GAX, glucuronoarabinoxylan; HG/HGA, homogalacturonan; i, interior crystalline cellulose; INADEQUATE, incredible natural-abundance double-quantum transfer experiment; MAS, magic-angle spinning; MLG, mixed-linkage glucan; PDSD, proton-driven spin diffusion; s, surface cellulose; SSNMR, solid-state NMR; WT, wild-type; XyG, xyloglucan.

Although the chemical structures and compositions of plant cell wall polymers are relatively well known, how these wall polymers form a 3D network to provide mechanical strength to the wall while allowing the wall to expand and grow is still poorly understood (Cosgrove, 2001, 2014). Molecular-level 3D structural information is difficult to obtain because of the insoluble nature of the cell wall and the amorphous nature of most wall polysaccharides except cellulose (Jarvis, 1992; Cosgrove, 2005). Thus, decades of cell wall structure characterization mainly involved chemical extractions followed by sugar analysis and microscopic imaging, which are limited by significant perturbation of the wall structure and insufficient spatial resolution (Mccann *et al.*, 1990, 1995; Talbott and Ray, 1992). *In vitro* binding assays have been used to measure the binding affinities between different wall polysaccharides, but they cannot reproduce the complex molecular interactions in the native wall after biosynthesis. VanderHart and Atalla pioneered the use of ^{13}C solid-state NMR (SSNMR) spectroscopy to characterize purified cellulose in higher plants (Atalla and VanderHart, 1984, 1999). From the ^{13}C chemical shifts, they resolved two cellulose allomorphs, I_α and I_β. Recently, advanced 2D correlation SSNMR techniques were used to definitively assign these ^{13}C chemical shifts and obtain ^{1}H chemical shifts in bacterial and tunicate cellulose (Kono *et al.*, 2003; Kono and Numata, 2006). These data indicate that the anhydroglucose residues in the two cellulose allomorphs have distinct conformations and are distributed differently in the glucan chains. SSNMR has also been used to investigate polysaccharide structures in secondary cell walls (Bardet *et al.*, 1997; Dupree *et al.*, 2015), protein cross linking in soybean cell walls (Cegelski *et al.*, 2010), and effects of hydration on polysaccharide mobility in onion cell walls (Hediger *et al.*, 1999, 2002). However, these SSNMR studies did not give information on cellulose interactions with matrix polysaccharides in primary cell walls.

Recently, we introduced 2D and 3D correlation SSNMR for investigating the intermolecular interactions of polysaccharides in near-native, hydrated plant primary cell walls (Dick-Perez *et al.*, 2011). By labelling whole plants with ^{13}C, we obtained sufficient sensitivity to conduct multidimensional correlation SSNMR experiments, which are necessary for resolving the signals of multiple wall polysaccharides. In this way, we obtained site-specific information about the conformation, dynamics, water interaction, and intermolecular contacts of the macromolecules in near-native plant cell walls. In this paper, we review key results from these multidimensional correlation SSNMR data. We show that there are relatively few cellulose–xyloglucan cross peaks but many cellulose–pectin cross peaks in *Arabidopsis* cell walls, which revise the conventional 'tethered-network' model of the cell wall and suggest instead a single cohesive network in which cellulose contacts both pectins and xyloglucan (Dick-Perez *et al.*, 2011; Wang *et al.*, 2012). Similarly, we observed cellulose-GAX cross peaks in the cell wall of the model grass *Brachypodium*, which provide new insight into polysaccharide interactions in grass cell walls. The major findings of these SSNMR studies are summarized in Table 1.

The C4 chemical shifts of most native celluloses exhibit two resolved bands centred at 89 ppm and 85 ppm, which have long been attributed to interior and surface chains of the microfibril, respectively (Earl and VanderHart, 1981). The relative intensities of these surface and interior cellulose peaks were recently used together with X-ray diffraction and computational modelling to constrain the cross-sectional area of cellulose microfibrils in plants, resulting in structural models with as few as 15 chains and as many as 25 chains (Newman *et al.*, 1994, 1996, 2013; Kennedy *et al.*, 2007; Fernandes *et al.*, 2011; Thomas *et al.*, 2013). These estimates are much smaller than the original 36-chain model proposed based on the hypothesized number of cellulose–synthase proteins in the plasma membrane (Scheible *et al.*, 2001; Taylor, 2008; Guerriero *et al.*, 2010), and the 18-chain model was particularly guided by emerging biochemical data indicating the stoichiometry of the different cellulose synthases in hexameric rosettes and computational modelling of the cellulose synthase structure (Sethaphong *et al.*, 2013; Hill *et al.*, 2014). In this paper, we provide the first quantitative analysis of the intensities of interior and surface cellulose C4 signals in

Table 1. *SSNMR studies of primary cell walls by Hong research group*

Major findings	Key experiments	References
There are limited XyG-cellulose contacts but extensive pectin-cellulose contacts in *Arabidopsis* cell walls.	DQF, INADEQUATE, DIPSHIFT, 3D CCC	Dick-Perez *et al.* (2011)
Partial depectination rigidifies the remaining wall polymers.	PDSD, ^{13}C–T_1, ^{1}H–$T_{1\rho}$	Dick-Perez *et al.* (2012)
25–50% of the cellulose surface is surrounded by pectins.	PDSD buildup analysis, RFDR	Wang *et al.* (2012)
Cellulose crystallinity is reduced in cesa1^{aegeus}/cesa3^{ixr1-2} mutant.	CP, DP, INADEQUATE	Harris *et al.* (2012)
Expansin binds XyG-enriched regions of cellulose microfibrils to loosen the cell wall.	Dynamic nuclear polarization, Protein-edited spin diffusion	Wang *et al.* (2013)
GAX and cellulose have sub-nanometre spatial contacts in *Brachypodium* cell walls.	Short-CP PDSD, ^{13}C–T_1, ^{1}H–$T_{1\rho}$	Wang *et al.* (2014)
Use water to probe the structure of intact and digested walls.	Water-polysaccharide spin diffusion	White *et al.* (2014)
Intermolecular cross peaks can be selectively detected in a new 2D ^{13}C correlation experiments.	T_1-compensated PDSD	Wang *et al.* (2015b)
Cellulose-pectin spatial contacts are inherent in the primary walls, independent of the hydration history. Never-dried and rehydrated walls show the same cellulose–pectin cross peaks.	^{13}C–^{1}H MELODI-HETCOR	Wang *et al.* (2015a)

several plant primary cell walls. The resulting, more accurate, intensity ratios indicate a minimum number of 24 chains in both dicot and grass primary cell wall cellulose microfibrils.

Plant cell wall ^{13}C labelling for magic-angle-spinning SSNMR

The main requirement for 2D and 3D ^{13}C magic-angle-spinning (MAS) SSNMR studies of plant cell walls is ^{13}C enrichment of the cell wall. This ^{13}C labelling gives the necessary sensitivity to correlate and resolve the signals of many polysaccharides and proteins. We labelled *Arabidopsis* and *Brachypodium* primary cell walls by growing the plants in liquid culture containing ^{13}C-labelled glucose in the dark. By restricting the growth period to 2 weeks, we produced chiefly primary cell walls with negligible amounts of secondary cell walls, as confirmed by the lack of lignin signals in the SSNMR spectra (Dick-Perez *et al.*, 2011). Whole seedlings were harvested and intracellular molecules and starch were removed by SDS, sodium metabisulphate, and amylase. All cell wall samples for these SSNMR studies were well hydrated (40–80 weight% water): the first samples involved freeze–drying of the wall followed by rehydration (Dick-Perez *et al.*, 2011; Wang *et al.*, 2012), while subsequent samples were never dried (Wang *et al.*, 2014; White *et al.*, 2014). Our recent comparison of the rehydrated and never-dried cell walls found that polysaccharides ^{13}C chemical shifts, nuclear-spin relaxation times, and intermolecular cross peaks are indistinguishable (Wang *et al.*, 2015a), indicating that the molecular-level structure and dynamics of wall polysaccharides are reproducible and reversible upon rehydration. Comparison of the quantitative NMR spectra with sugar analysis results (Dick-Perez *et al.*, 2011; White *et al.*, 2014) also indicates that the ^{13}C labelling is relatively uniform for all wall polysaccharides.

^{13}C resonance assignment and the nature of cross peaks in multidimensional SSNMR spectra

The first step in extracting information from the 2D and 3D SSNMR spectra is to resolve and assign the ^{13}C chemical shifts of the polysaccharides and proteins. We achieved this using a combination of four correlation NMR techniques: 1) 2D ^{13}C-^{13}C double-quantum to single-quantum correlation mediated by through-bond ^{13}C-^{13}C J-coupling. This experiment is called J-INADEQUATE (Bax *et al.*, 1980; Lesage *et al.*, 1997); 2) 2D ^{13}C-^{13}C ^{1}H-driven spin diffusion experiments called PDSD or DARR (Takegoshi *et al.*, 2001); 3) Double-quantum-filtered (DQF) 2D ^{13}C-^{13}C correlation experiment using homonuclear dipolar recoupling sequences (Hohwy *et al.*, 1999); 4) 3D ^{13}C-^{13}C-^{13}C correlation experiment mediated by ^{13}C spin diffusion (Li *et al.*, 2010). The J-INADEQUATE experiment exhibits cross peaks only between bonded ^{13}C spins, because the polarization is transferred via the electrons in the covalent bond, while the other three experiments exhibit cross peaks between carbons that are close in space, because polarization transfer is mediated by distance-dependent dipolar couplings. Thus, cross peaks from experiments 2) to 4) can occur between directly bonded or non-bonded carbons. For carbons in a uniformly ^{13}C-labelled sugar residue, relayed dipolar transfer through multiple bonds is highly efficient. Thus, a C1–C3 cross-peak, for example, is most likely mediated by relayed C1–C2 and C2–C3 dipolar transfer instead of direct C1–C3 dipolar transfer. The DQF correlation experiment differs from the spin diffusion experiments in that the former mostly exhibits one-bond and two-bond cross peaks, so that the spectra are relatively simple, while the latter can exhibit cross peaks between more distant carbons. To detect long-range ^{13}C-^{13}C distances up to 1 nm, one can increase the spin diffusion mixing time. The intensity buildup of cross peaks with the mixing time contains semi-quantitative information about internuclear distances. To better resolve long-range cross peaks with high structural content from short-range cross peaks that are mainly useful for resonance assignment, we introduced a relaxation-compensated PDSD technique, which produces a difference spectrum that shows only intermolecular cross peaks (Wang *et al.*, 2015b). Further development of SSNMR methods will be desirable for resolving and detecting intermolecular contacts between different wall polymers.

These 2D and 3D ^{13}C correlation NMR spectra allowed us to type-assign most ^{13}C signals of the common monosaccharides, namely Glc, Ara, GalA, GlcA, Xyl, Rha, and Gal, in the primary walls of *Arabidopsis* (Dick-Perez *et al.*, 2011), *Brachypodium* (Wang *et al.*, 2014), and *maize* (unpublished data). For the same type of monosaccharide, the ^{13}C chemical shifts can vary due to different sugar conformations, linkages, and hydrogen bonding patterns. For example, nine types of arabinose signals were resolved in *Brachypodium* cell walls, which can be assigned to different arabinose linkages in GAX and arabinan (Wang *et al.*, 2014). So far, the resolved polysaccharide-specific signals include all six glucose carbons of interior and surface cellulose (Wang *et al.*, 2012), all five ^{13}C signals of Xyl in XyG, all Ara signals of arabinan (Dick-Perez *et al.*, 2011), and all signals of Xyl, GlcA, and ferulic acid in GAX (Wang *et al.*, 2014). The Glc backbone and Gal sidechain of XyG are incompletely resolved due to signal overlap from surface cellulose and galactan, respectively. In addition, GalA signals are often used to denote pectin backbones, but their originating polysaccharides, HG and RG, cannot yet be distinguished. Polysaccharide-specific isotopic labelling will be useful to further resolve these signals.

Higher magnetic fields significantly enhance the resolution of the cell wall NMR spectra. To date, the highest field strength we have used for plant cell walls is 21.1 Tesla, corresponding to a ^{1}H Larmor frequency of 900 MHz. At this field strength, at least two types of crystalline cellulose signals have been observed (Wang *et al.*, 2012) and dramatic improvement of spectral resolution is seen for matrix polysaccharides. For example, Fig. 1 compares the 2D J-INADEQUATE spectra of the same *Arabidopsis* primary cell wall sample at 400, 600, and 900 MHz. The ^{13}C linewidths of matrix polysaccharides are 0.7–1.4 ppm at 400 MHz, 0.5–1.1 ppm at 600 MHz, and only 0.2–0.5 ppm at 900 MHz. The cellulose spectral resolution is also substantially improved: the linewidths are ~2 ppm at low fields but narrow to 0.7–1.0 ppm at 900 MHz. This

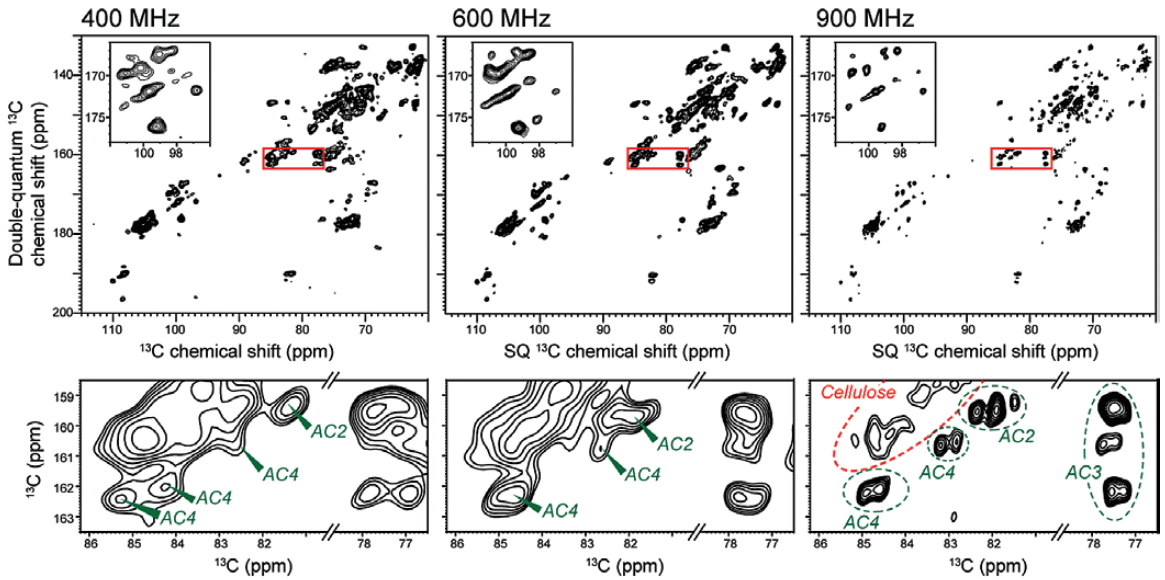

Fig. 1. 2D ^{13}C-^{13}C J-INADEQUATE spectra of never-dried *Arabidopsis* cell walls at room temperature, correlating double-quantum (DQ) and single-quantum (SQ) ^{13}C chemical shifts. The spectra were measured at 400, 600, and 900 MHz. Insets magnify the C1 region of the spectra to indicate the resolution enhancement by higher magnetic fields. The bottom row amplifies the C2–C4 region of arabinose, where high magnetic fields significantly improve the resolution of multiple forms of arabinose.

line narrowing indicates that the ^{13}C linewidths of uniformly ^{13}C-labelled cell walls have a substantial homogeneous contribution due to residual dipolar couplings to ^{1}H and ^{13}C-^{13}C J-couplings, which becomes less important at higher magnetic fields. Using the C1 region of the 2D J-INADEQUATE spectra as an example, the 900 MHz spectrum resolves at least 14 peaks while the 400 MHz spectrum resolves only ~10 peaks (Fig. 1). In addition, the 900 MHz spectrum resolves three types of AC2 and four types of AC4, while the spectra measured at lower fields only exhibit one broad AC2 peak and one or two AC4 peaks, partially overlapped with cellulose signals. With the enhanced resolution at high fields, we can unambiguously resolve signals that are only 0.2–0.3 ppm apart. Further increase of the NMR field strengths to 1.0 GHz and beyond is expected to provide even more benefit for obtaining finer structural details of wall polysaccharides.

The challenge of resolving the polysaccharide signals of native cell walls is also met by exploiting the mobility difference between cellulose and matrix polysaccharides: cellulose is largely immobilized except for the C6 hydroxymethyl group, whereas pectins and hemicellulose are highly mobile with C–H bond order parameters of ~0.5 (Dick-Perez *et al.*, 2011; Wang *et al.*, 2014). This mobility difference allows us to selectively detect the signals of rigid or mobile polysaccharides in separate spectra. For example, the mobile GAX in the *Brachypodium* primary wall were selectively detected in the 2D J-INADEQUATE spectra measured with direct polarization (DP), and the large number of narrow ^{13}C signals has been assigned to five different Xyl and nine different Ara types, indicating the diverse linkages and substitution patterns of GAX in grass primary walls (Wang *et al.*, 2014). ^{13}C-^{1}H dipolar dephasing has also been used to suppress the signals of rigid cellulose and detect only those of mobile matrix polysaccharides (Komatsu and Kikuchi, 2013). Conversely, by using short ^{1}H-^{13}C cross polarization (CP) transfer, we have obtained ^{13}C spectra exhibiting only cellulose signals in the *Brachypodium* cell wall.

Intermolecular cross peaks of primary cell wall polysaccharides

The assignment of most polysaccharide ^{13}C chemical shifts allowed us to determine ^{13}C-^{13}C cross peaks that reflect intermolecular proximities. With mixing times of 1.5 s and shorter, a conservative estimate of the upper bound of ^{13}C-^{13}C distances is 10 Å. For the *Arabidopsis* cell wall, 3D and 2D spectra have been measured with spin diffusion mixing times of up to 300 ms and 1.5 s, respectively (Dick-Perez *et al.*, 2011; Wang *et al.*, 2012). These spectra yielded a number of unambiguous cross peaks between cellulose and pectins, for example, between the crystalline cellulose C4 chemical shifts of 89 ppm and the pectin chemical shifts of 101 ppm and 80 ppm (Fig. 2A). On the other hand, although hemicellulose was long thought to cover the surfaces of cellulose microfibrils, cross peaks between the two are few and ambiguous. The 3D spectra of the *Arabidopsis* wall showed a few cellulose cross peaks with the XyG backbone Glc and with Gal sidechains (Dick-Perez *et al.*, 2011), but no unambiguous signals between cellulose and xylose were detected. Further experiments that better resolve XyG signals will be useful for verifying the paucity of cellulose–hemicellulose cross peaks. However, the fact that even with partial resonance overlap, such cellulose–hemicellulose cross peaks are not abundant strongly suggests that XyG does not extensively coat the microfibril surface (Bootten *et al.*, 2004). Since *in vitro* assembly data showed that XyG has a stronger affinity for cellulose than pectins, these SSNMR data imply that *in vivo* wall assembly is quite different from *in vitro* assembly, and pectins and hemicellulose may compete for cellulose binding sites in ways that are not replicated *in vitro* (Wang *et al.*, 2015a).

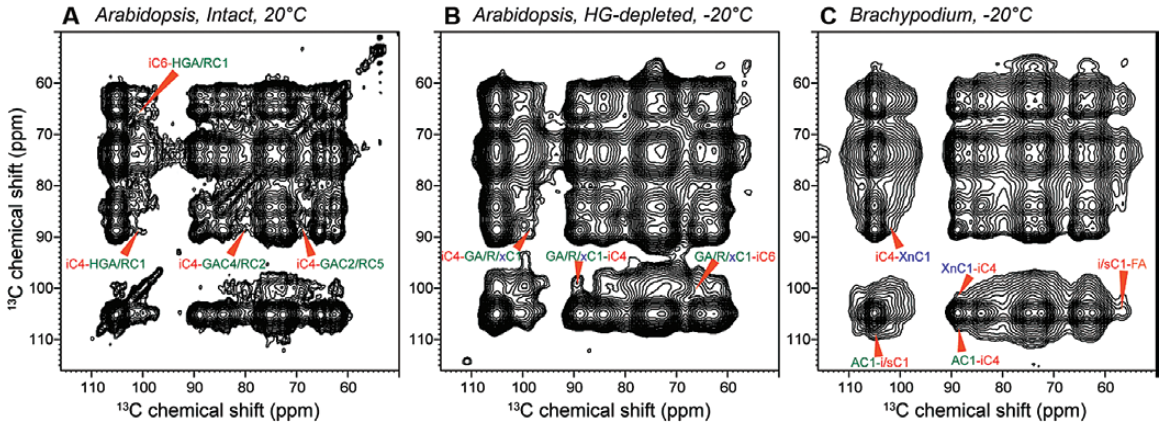

Fig. 2. 2D ^{13}C-^{13}C PDSD spectra of plant cell walls measured with 1.5 s spin diffusion mixing. (A) Intact *Arabidopsis* cell wall at 20 °C. (B) HG-depleted *Arabidopsis* cell wall at –20 °C. (C) *Brachypodium* cell wall at –20 °C. Cellulose–pectin cross peaks are observed in both intact and HG-depleted *Arabidopsis* cell walls, and cellulose–GAX cross peaks are detected in the *Brachypodium* sample.

It is noteworthy that most cellulose–pectin cross peaks observed in the intact cell wall are retained in a sample in which ~40% of HG had been extracted (Fig. 2A, B) (Wang *et al.*, 2015a). This means that the cellulose–pectin spatial contacts are not due to molecular crowding; rather, RG-I and some of the HG are responsible for contacting cellulose. These findings are consistent with the observation that cellulose–pectin cross peaks are also independent of hydration and temperature, and together suggest that the interactions between pectins and cellulose are specific, and some pectins may be entrapped inside or between the microfibrils (Wang *et al.*, 2015a). Therefore, pectins may play more important roles in wall biomechanics than depicted in the traditional tethered-network model. Indeed, recent biochemical data showed that arabinans and galactans interact strongly with cellulose (Zykwinska *et al.*, 2007), and XyG-deficient cell walls exhibit almost normal development as wild-type (WT) cell wall (Cavalier *et al.*, 2008).

The matrix polysaccharides of grass primary cell walls differ chemically from those of dicot primary walls (Carpita and Gibeaut, 1993; Carpita, 1996). In the 2-week-old *Brachypodium* primary walls, the main matrix polysaccharide is highly branched GAX (Wang *et al.*, 2014), and no MLG signals were detected. For this two-component cell wall, 2D ^{13}C correlation spectra exhibited many cellulose–GAX cross peaks, for example between Ara C1 (108.4 ppm) and interior cellulose C4 (88.3 ppm), and between Xyl C1 (102.0 ppm) and interior cellulose C4 (Fig. 2C). Although such GAX–cellulose spatial contact may not seem surprising given the fact that few other matrix polysaccharides are present, the data counter the conventional model that highly branched GAX chains cannot bind cellulose. An implication of this finding is that the cellulose microfibril has sufficient unevenness and surface disorder to accommodate the branched polysaccharides. Again, *in vitro* binding assays report only a small fraction (4–15%) of GAX binding to cellulose (Carpita, 1983), similar to the low-level of pectin–cellulose binding *in vitro*, but these results may systematically underestimate the *in vivo* intermolecular interactions in the wall.

Percentages of sugar residues at intermolecular interfaces

Since the cross-peak intensities at long mixing times reflect the percentage of a polysaccharide in nanometre contact with each other, we can estimate the percentages of sugar residues at intermolecular interfaces. Since each surface cellulose chain must be adjacent to one interior cellulose chain, the surface–interior cellulose cross-peak intensity in the 2D spectra serves as an internal control of the extent of intermolecular contacts between matrix polysaccharides and cellulose. We found that 25–50% of surface cellulose contacts pectins (Wang *et al.*, 2012). This is a very significant percentage not predicted by existing cell wall structural models. The extent of cellulose–XyG interaction cannot be accurately estimated because of insufficient resolution of the XyG backbone signals in the spectra.

A second approach for estimating the percentages of pectins and XyG that interact with cellulose is by detecting heterogeneous mobilities of the matrix polysaccharides. In both *Arabidopsis* and *Brachypodium* primary walls, cellulose backbone exhibits single-exponential decays for both ^{13}C spin-lattice (T_1) relaxation and ^{1}H rotating-frame spin-lattice relaxation ($T_{1\rho}$) (Dick-Perez *et al.*, 2011; Wang *et al.*, 2014), indicating that cellulose is uniformly rigid. In comparison, XyG and pectins in *Arabidopsis* show double-exponential relaxation where 40–60% of a highly mobile component coexists with a rigid component. The most likely interpretation of this bimodal dynamics is that two domains exist in each matrix polysaccharide: the rigid domain interacts with cellulose through van der Waals interaction, hydrogen bonding, or entrapment, while the mobile domain occupies the inter-fibrillar space. Interestingly, in both *Arabidopsis* and *Brachypodium* primary walls, the well resolved 65-ppm peak of interior cellulose C6 also exhibits bimodal relaxation, with the mobile component accounting for ~20% of the total intensity. This mobility could be explained by the freedom of C6 to rotate and change the C4–C5–C6–O6 torsion angle (Matthews *et al.*, 2006; Fernandes *et al.*, 2011) or by the flexibilities of the matrix polysaccharides that contact cellulose, which may influence the exposed C6 more than the embedded ring carbons.

Single network model of plant primary walls

The intermolecular cross peaks in the 2D and 3D ^{13}C correlation spectra support a single network model of primary cell walls, in which both pectins and hemicellulose interact with cellulose microfibrils. This conclusion is supported by a recent hydration study that found that removal of Ca^{2+} ions that crosslink HG slowed down water ^{1}H spin diffusion to both pectins and cellulose (White *et al.*, 2014), indicating that cellulose interacts intimately with pectins. This structural conclusion also found support from recent biomechanical assays showing that the majority of XyG does not have load-bearing function, since endoglucanases that hydrolyse only XyG or only cellulose do not cause wall creep. Instead, an endoglucanase that simultaneously cuts XyG and cellulose loosens the wall, thus only a small fraction of XyG binds cellulose as load-bearing tethers (Park and Cosgrove, 2012a, b). Intriguingly, these cellulose-XyG 'biomechanical hotspots' have been recently found to be the site of expansin binding using ^{13}C spin diffusion NMR (Wang *et al.*, 2013).

Lateral heterogeneity of cellulose conformations in the microfibril from 2D SSNMR spectra

Multidimensional ^{13}C SSNMR not only provides information on the 3D architecture of the cell wall, but also constrains the cross-sectional area of cellulose microfibrils. The C1, C4, and C6 chemical shifts of cellulose have long been known to be diagnostic of cellulose crystallinity and allomorphs (Atalla and VanderHart, 1984, 1999; Horii *et al.*, 1987). For our analysis below, we assign the C4 and C6 chemical shifts of 89 and 65 ppm to interior crystalline glucan chains, and the 85 and 62 ppm peaks to surface chains with partial disorder. The 89/65 ppm interior glucan signals are well resolved from all other polysaccharides' signals, thus they are unambiguous indicators of cellulose. The possibility that the 85/62 ppm chains may reside inside the microfibril instead of on the surface is considered low, because the 85/62 ppm peaks have strong cross peaks with matrix polysaccharides and water (Fernandes *et al.*, 2011; Wang *et al.*, 2012; White *et al.*, 2014) and exhibit large-amplitude dynamics (Dick-Perez *et al.*, 2011; Wang *et al.*, 2014). Longitudinal disorder of interior glucan chains has been estimated at only 4–5 residues for every 300 residues (Nishiyama *et al.*, 2003a), thus it should not significantly affect the extracted ratio of surface:interior chain numbers.

Fig. 3 shows the 2D ^{13}C-^{13}C PDSD spectrum of never-dried *Brachypodium* cell walls at 20 °C (Wang *et al.*, 2014). The ^{13}C magnetization was created using a short ^{1}H-^{13}C CP contact time of 35 μs, which suppressed the signals of mobile polysaccharides and gave a predominantly cellulose spectrum in the indirect dimension. A long ^{13}C spin diffusion mixing time of 3.0 s was applied to transfer the ^{13}C magnetization to polysaccharides within ~1 nm of the cellulose. Interestingly, despite the long mixing time, the ^{13}C cross sections of interior and surface cellulose are not identical (Fig. 3B), with the difference spectrum corresponding to that of pure crystalline cellulose. Long mixing time PDSD spectra were also measured at low temperature (−20 °C) to freeze molecular motion and with regular CP contact times to detect all polysaccharide signals. The resulting surface and interior cellulose cross sections still retain their different intensity distributions (Wang *et al.*, 2014). These results indicate that some interior glucan chains are separated from the surface chains by more than the distance reach of ^{13}C spin diffusion. Thus, there are two types of interior cellulose chains: a core (c) fraction that is not in direct contact with the surface, and a bound (b) fraction (Fig. 3C). This result dovetails an earlier structural model based on spectral deconvolution, which suggested the presence of a para-crystalline layer between the microfibril surface and the crystalline core (Larsson *et al.*, 1999). The C6 of the two interior cellulose fractions resonates at slightly different chemical shifts, 65.5 ppm for the core cellulose and

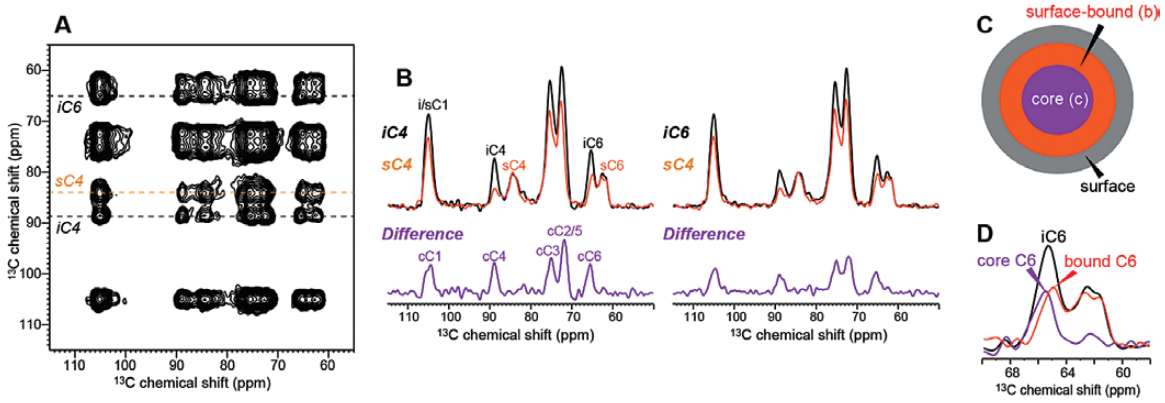

Fig. 3. (A) 2D ^{13}C-^{13}C PDSD spectrum of *Brachypodium* cell wall with a 3.0 s mixing. The spectrum was measured at 20 °C with a short ^{1}H-^{13}C CP contact time of 35 μs to suppress the signals of mobile GAX. (B) Representative cross sections of interior cellulose (black) and surface cellulose (orange). The different intensity patterns indicate that ^{13}C magnetization has not equilibrated between interior and surface cellulose. The difference spectra (purple), obtained after normalizing the two cross sections by the sC4 peak, correspond to core cellulose chains that are inaccessible to the surface. (C) Illustration of the cellulose microfibril structure, where interior cellulose consists of a surface-bound fraction and a core fraction. (D) The two types of interior cellulose chains have slightly different C6 chemical shifts.

64.8 ppm for the surface-bound interior cellulose (Fig. 3D), suggesting that the hydroxymethyl conformation depends on the location of the interior chains, with the core cellulose C6 chemical shift corresponding to that of a *trans-gauche* (tg) conformer (Vietor *et al.*, 2002). The *Brachypodium* result is reproduced in the *Arabidopsis* cell wall (Fig. 4), which also exhibits different surface and interior cellulose cross sections at long mixing times, with the difference spectrum corresponding to the signals of crystalline cellulose. Therefore, cellulose microfibrils in both grass and dicot primary walls are sufficiently large to contain three layers of glucan chains.

The core cellulose has two resolved cC1 peaks at 105.5 and 104.0 ppm (Table 2), which resemble the C1 chemical shifts of I_β cellulose (Kono *et al.*, 2003). The C3, C5, and C6 chemical shifts of core cellulose are also similar to those of I_β cellulose. However, no doublet is observed for C6, as expected for I_β cellulose. We attribute this absence to insufficient resolution since the two I_β C6 chemical shifts differ by only 0.6 ppm based on tunicate cellulose data (Table 2) (Kono *et al.*, 2003; Kono and Numata, 2006). The I_β allomorph contains two types of magnetically inequivalent anhydroglucose residues, which are not directly linked in the same chain but are located in different chains (Kono and Numata, 2006) and perhaps even in alternating sheets (Nishiyama *et al.*, 2002; Jarvis, 2003). It is well known that the I_α allomorph dominates in bacterial and algae while the I_β allomorph dominates in the secondary cell walls of higher plants (Atalla and VanderHart, 1984). The iC4 chemical shifts of *Arabidopsis* primary walls suggest that both I_α and I_β allomorphs are present (Newman *et al.*, 1996), with I_β being slightly more abundant. More detailed structural information of the primary-wall cellulose will require more advanced experiments that resolve the ^{13}C chemical shifts of surface cellulose and matrix polysaccharides and that relate ^{13}C chemical shifts to direct conformational parameters such as torsion angles and distances.

The number of glucan chains in cellulose microfibrils from quantitative ^{13}C SSNMR spectra

The number of glucan chains in plant cellulose microfibrils has been estimated from the relative intensities of surface and interior cellulose C4 peaks in the SSNMR spectra (Newman *et al.*, 1994, 1996; Kennedy *et al.*, 2007). Since ^{13}C spectra also contain matrix polysaccharide signals that partly overlap

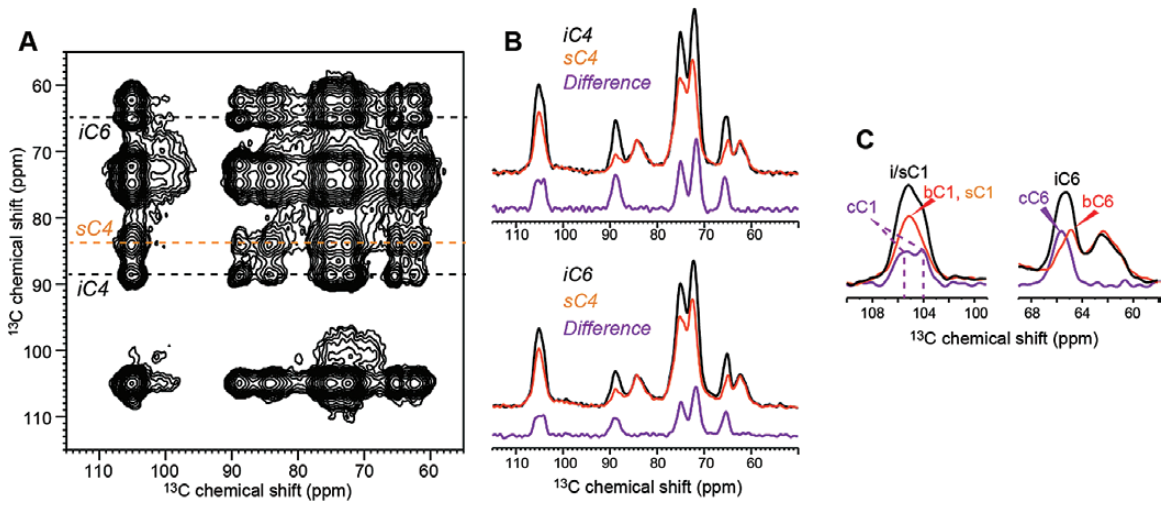

Fig. 4. 2D ^{13}C-^{13}C PDSD spectrum of *Arabidopsis* cell walls with a 1.5 s mixing time. The spectrum was measured at –20 °C under 9 kHz MAS. (A) 2D spectrum. (B) Representative cellulose cross sections of interior and surface cellulose exhibit different intensity patterns. The difference spectra (purple) were obtained after normalizing the two spectra by the sC4 peak. The surface cellulose cross section has contribution from Ara and XyG backbone, but the difference spectra mainly show signals of interior cellulose. (C) C1 and C6 regions of the cellulose cross sections and the difference spectra. Core cellulose C1 shows two peaks at 105.5 ppm and 104.1 ppm, and core cellulose C6 (cC6) exhibits a 0.3 ppm downfield shift from the average interior cellulose C6 (iC6) and 0.6 ppm downfield shift from the surface-bound interior cellulose (bC6).

Table 2. *Cellulose chemical shifts observed in 1D and 2D ^{13}C SSNMR spectra here and in the literature by multidimensional correlation NMR*

The chemical shifts of the core cellulose that are similar to those of the I_β allomorph are underlined.

Organisms	Form	C1 (ppm)	C2 (ppm)	C3 (ppm)	C4 (ppm)	C5 (ppm)	C6 (ppm)	Sources
Arabidopsis	Core	105.5/104.1	71.7	75.0	88.8	71.7	65.6	1.5 s PDSD
Brachypodium	Core	105.5/104.3	71.9	75.0	88.9	71.9	65.5	3.0 s PDSD
Cladophora	I_α	105.0	71.6	74.7	90.0	70.1	65.2	Kono *et al.* (2003)
		105.0	70.1	73.9	89.1	72.6	65.2	Kono *et al.* (2003)
Tunicate	I_β	106.1	71.3	74.9	88.0	70.6	65.6	
		104.0	71.0	74.2	88.9	72.2	65.0	

with the surface cellulose peaks, Newman and coworkers used nuclear-spin relaxation to edit the ^{13}C spectra: linear combinations of CP spectra with and without relaxation filters resulted in predominantly cellulose or predominantly matrix polysaccharide sub-spectra. The cellulose sub-spectrum indicated a crystallinity of 0.37–0.44, which translates to a surface to interior chain number ratio (s:i) of 1.3–1.7. This range corresponds to an average number of 23 chains in the microfibril (Newman *et al.*, 1994, 1996).

Two assumptions in this relaxation-filtered NMR approach are that surface cellulose has the same dynamic property as interior cellulose and that matrix polysaccharides are fully removed by the relaxation filters due to their fast dynamics. However, recent measurements of spin-diffusion-free ^{1}H $T_{1\rho}$ relaxation times showed that in hydrated primary cell walls, the surface cellulose is more mobile than interior cellulose, while a non-negligible fraction of matrix polysaccharides is relatively rigid, presumably due to their contact with the cellulose microfibril (Dick-Perez *et al.*, 2011; Wang *et al.*, 2012). Thus, the signals of the rigid fraction of matrix polysaccharides may be difficult to suppress completely in the CP spectra. As a result, the relaxation-filtered ^{13}C spectra may neither represent only the cellulose signals nor capture all cellulose intensities. In addition, ^{13}C CP spectra are inherently non-quantitative unless specially designed pulse sequences are used (Johnson and Schmidt-Rohr, 2014), because the CP process is affected by motion and nuclear-spin relaxation, and generally favour the detection of rigid molecules while under-representing dynamic polysaccharides.

Quantitative intensities of surface and interior cellulose are most reliably obtained from ^{13}C DP spectra measured with long recycle delays. We measured and compared such quantitative ^{13}C spectra of several plants using recycle delays of 15–25 s (Fig. 5), which are sufficiently long to equilibrate the ^{13}C magnetization of these uniformly ^{13}C-labelled cell walls, whose T_1 relaxation times have been measured to be 1–4 s

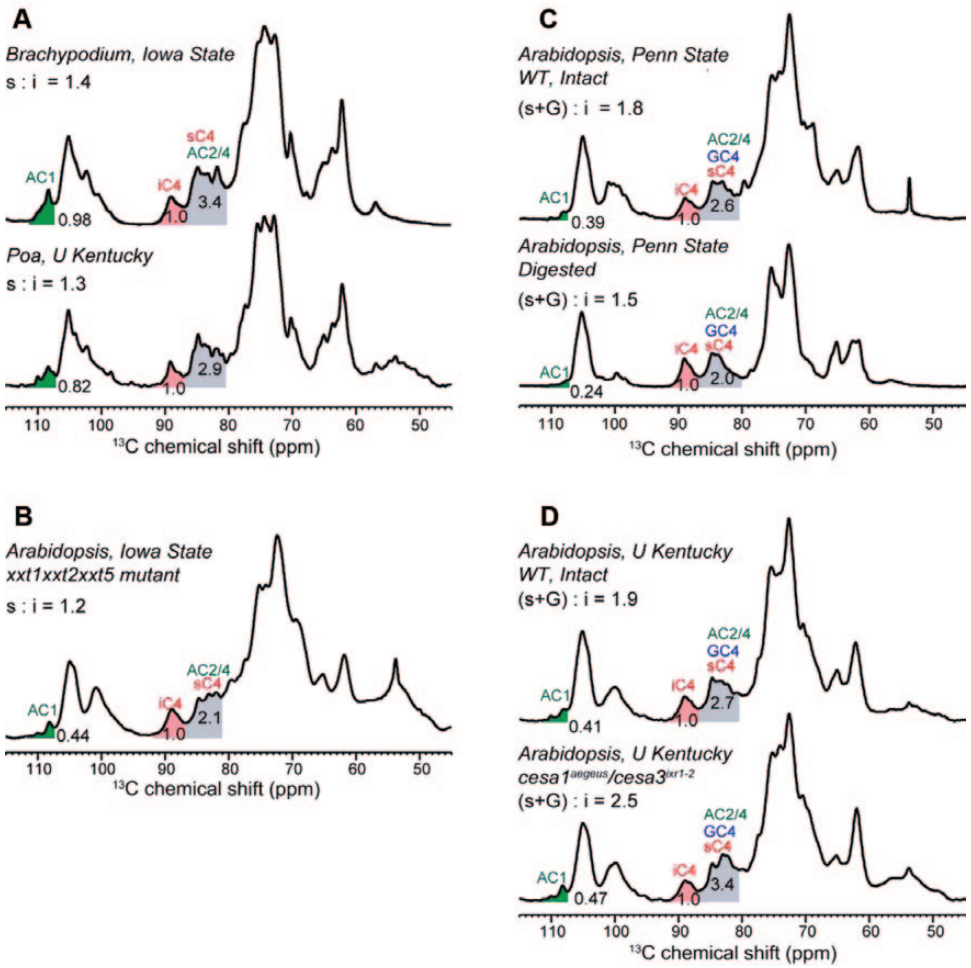

Fig. 5. 1D quantitative ^{13}C DP spectra of ^{13}C-labelled primary cell walls at ambient temperature. All spectra were measured with recycle delays of 15 to 25 s, except for the *xxt1xxt2xxt5* sample, which was measured with recycle delays of 10 s. (A) Spectra of grass cell walls with negligible amounts of XyG. Two grasses, *Brachypodium distachyon* (top) and *Poa annua* (bottom), were measured. The Ara C1 (AC1) and interior cellulose C4 (iC4) peaks are highlighted in green and red, respectively. The mixed peaks of surface cellulose C4 and Ara C2 and C4 are shaded in grey. The integrated intensities were used to calculate the surface:interior cellulose ratio (s:i). Grass has a small s:i ratio of 1.3–1.4, indicating at least 24 glucan chains (see Fig. 6). (B) A triple mutant of *Arabidopsis thaliana* with negligible XyG. (C) Intact (top) and digested (bottom) *Arabidopsis* cell walls. (D) WT and CESA mutant of *Arabidopsis*. The integration regions are 111.8–107.2 ppm for AC1, 92.0–86.8 ppm for iC4, and 86.8–80.4 ppm for the mixed peak of sC4 and matrix polysaccharides. The boundary of the mixed peak changed to 81.0 ppm for the *xxt1xxt2xxt5* mutant cell wall to avoid overlap with a strong pectin peak at 79.6 ppm.

(Dick-Perez *et al.*, 2011; Wang *et al.*, 2014). These ^{13}C T_1 values are much shorter than those of unlabelled cell walls because ^{13}C spin diffusion in the labelled samples is much more efficient and equilibrates the short T_1's of dynamic functional groups with the long T_1's of rigid functional groups. In comparison, the majority of the plant cell wall SSNMR literature involved unlabelled cell wall samples with much longer ^{13}C T_1 relaxation times, thus the quantitative ^{13}C DP experiment was not conducted due to its prohibitively low sensitivity, and most SSNMR analysis of the surface and interior glucan chain numbers relied on non-quantitative CP spectra.

In total, we examined the ^{13}C DP spectra of two grass cell walls and five *Arabidopsis* cell walls. Most cell walls were never dried during preparation, except for the *xxt1xxt2xxt3* mutant of *Arabidopsis* and samples prepared at the University of Kentucky, which were rehydrated samples (Table 3) (Dick-Perez *et al.*, 2011; Harris *et al.*, 2012; White *et al.*, 2014). We use the 86.8–80.4 ppm range to represent the surface cellulose C4 and unresolved matrix polysaccharide ^{13}C signals, the 92.0–86.8 ppm range to represent the interior cellulose C4 intensity, and the 111.8–107.2 ppm range to represent the Ara C1 intensity. The *Brachypodium* cell wall contains negligible amounts of XyG, thus the intensity analysis is straightforward. We integrated the interior cellulose C4 (iC4) peak, the Ara C1 peak, and the mixed peak of surface cellulose C4 (sC4), Ara C2 and C4 (Fig. 5A). Since the resolved Ara C1 peak indicates the intensity of a single carbon in Ara, subtraction of twice this intensity from the 86.8–80.4 ppm band yields the intensity of pure surface cellulose C4. In this way, we obtained an s:i ratio of 1.4 for *Brachypodium* cellulose. Similarly, an s:i ratio of 1.3 was found for the *Poa annua* cellulose (Brabham *et al.*, 2014). Spectral deconvolution based on the chemical shifts resolved in 2D ^{13}C-^{13}C correlation spectra yielded very similar s:i ratios with an experimental uncertainty of ±0.1.

For WT *Arabidopsis*, the surface cellulose intensities require more care to quantify because of the significant amount of XyG in the wall. We first examined the spectrum of the XyG-depleted *xxt1xxt2xxt5* mutant. The s:i ratio was found to be 1.2, in good agreement with the ratios of the grass cell walls. For WT *Arabidopsis* walls, the XyG backbone glucose C4 and the surface cellulose C4 signals are unresolved, thus we report the (s+G):i ratio. Intact walls prepared at Penn State University and the University of Kentucky gave (s+G):i ratios of 1.8–1.9 (Fig. 5C, D). When the majority of matrix polysaccharides were digested by sequential treatments with CDTA, Na_2CO_3, XEG, Cel12A, and 1 M NaOH (White *et al.*, 2014), the intensity ratio decreased to 1.5. Since residual matrix polysaccharides are still present in this digested sample, this value is an upper bound to the s:i ratios in intact WT *Arabidopsis* walls. Taken together, the s:i ratios of both grass and dicot primary walls (Table 3) span a range of 1.2–1.5, with an estimated error bar of ±0.1. For the reverse-engineered *Arabidopsis* mutant cesa1^{aegeus}/cesa3^{ixr1-2}, a much larger (s+G):i value of 2.5 was found. This was attributed to the significantly higher percentages of matrix polysaccharides in this mutant plant in response to the reduced crystallinity of cellulose (Harris *et al.*, 2012).

In modelling the number of glucan chains in the microfibril based on these quantitative s:i ratios, we assume that the number of glucan chains in adjacent planes varies by one and the chain numbers are symmetric with respect to the centre of the microfibril (Fig. 6). Smaller microfibrils have larger s:i ratios (Supplementary Fig. S1, available at *JXB* online) but models with different numbers of chains sometimes have similar s:i ratios due to different packing geometries (Supplementary Fig. S2, available at JXB online). For s:i ratios of 1.2–1.5, we found chain numbers of 36–24. If we use an s:i ratio of 1.3 as the average value for primary-wall cellulose, then the average number of glucan chains is 28. If we impose the constraint that the chain number is an integer multiple of 6 due to the hexameric structure of cellulose synthase (Herth, 1983; Endler and Persson, 2011), then the most likely chain numbers are 24 and 30. However, irregular microfibril cross sections with other chain numbers should be considered possible at this point. In comparison, small microfibril models with 18 or fewer chains correspond to s:i ratios of >2.0, which deviates from the measured data well beyond the experimental uncertainty, and thus can be excluded. Fig. 6B also shows that small microfibrils with 18 chains or fewer do not have a core domain, instead all interior chains contact the surface chains, which is inconsistent with the long mixing time 2D spectra shown in Figs 3 and 4. Thus, both the quantitative ^{13}C spectra and the 2D PDSD spectra indicate that the cellulose microfibrils in plant primary walls must be sufficiently large to contain at least 24 chains.

TEM, atomic force microscopy, X-ray scattering, and SSNMR data of plant primary walls generally indicate that the lateral dimension of the cellulose microfibrils is 2–5 nm (Guerriero *et al.*, 2010). In terms of the number of glucan chains, the earliest proposal of 36 chains based on the hypothesized number of cellulose synthase subunits in the rosette structure is now widely considered an over-estimate. Instead, recent proposals have shifted to the other extreme of very small microfibrils containing only 18 chains. The most influential study was based on a joint analysis of wide-angle X-ray scattering (WAXS) and SSNMR data of mung bean cell walls (Newman *et al.*, 2013), in which the WAXS data was deconvoluted using computer-simulated diffractograms of various cellulose models containing 18, 24, or 36 chains with different disorder. These models were simultaneously constrained by the NMR-derived crystallinity factor, X, which is directly related to the s:i ratio. The joint analysis suggested that a mixture of 18-chain microfibrils with irregular shapes and twinning best reproduced the WAXS and SSNMR data. It is of interest to assess the uncertainties in this analysis. First, the cross section shape factor, K, used in calculating the number of (200) planes in the microfibril is assumed to be 0.9 but can vary from 0.84 to 1.0. Using a higher K would increase the number of (200) planes and hence the number of chains. Second, the SSNMR constraint of X=0.37 corresponds to a large s:i ratio of 1.8, which is inconsistent with the quantitative s:i ratios found here. This large X most likely results from incomplete subtraction of the matrix polysaccharide intensities from the 87–80 ppm band. If s:i ratios of 1.2–1.5 were used (X: 0.45–0.40), and the K value is allowed to vary from

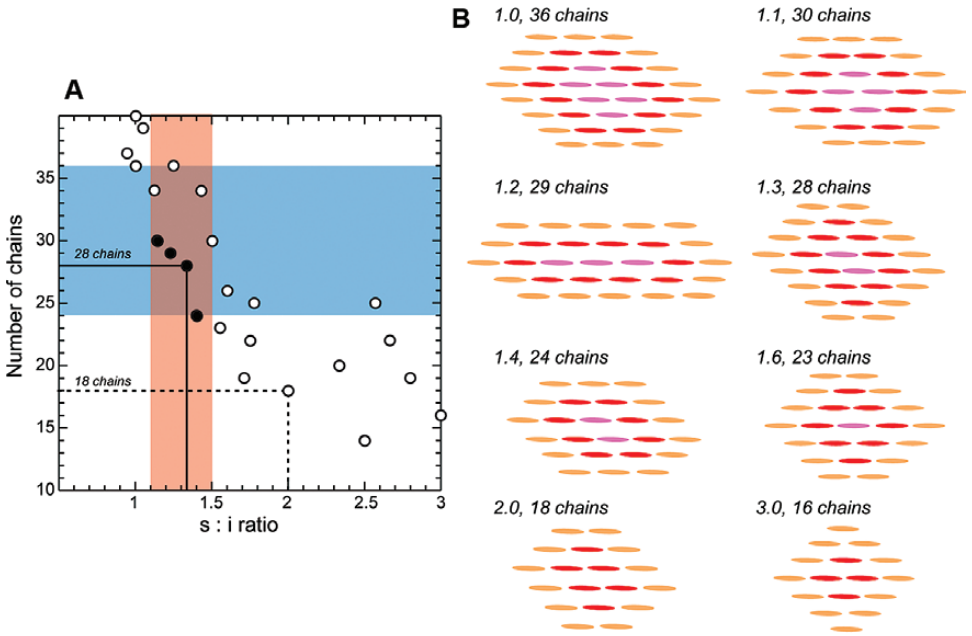

Fig. 6. Number of glucan chains in cellulose microfibrils as a function of the s:i ratio. The minimum number of glucan chains for s:i values of 1.1, 1.2, 1.3, 1.4, and 1.5 are 30, 29, 28, 24, and 30, respectively (filled circles). (B) Representative cellulose microfibril cross sections with different s:i ratios. For each model, glucan chains from core cellulose (magenta), surface-bound cellulose (red), and surface cellulose (orange) are depicted. Structural models with 18 or fewer chains correspond to s:i ratios of 2.0 or higher and lack core cellulose, which are inconsistent with the experimental data.

Table 3. *Surface to interior cellulose number ratios of various primary cell walls from ^{13}C quantitative DP spectra and short-CP spectra*

Sample	Preparation	Experiment	Peaks	Ratio
Brachypodium	Iowa state, never-dried	Quantitative DP	s:i	1.4
		Short CP	s:i	1.2
Poa annua	U Kentucky, rehydrated	Quantitative DP	s:i	1.3
Arabidopsis, xxt1xxt2xxt5	Iowa state, rehydrated	Quantitative DP	s i	1.2
Arabidopsis, WT, intact	Penn state, never-dried	Quantitative DP	(s+G):i	1.8
		Short CP	(s+G):i	1.5
Arabidopsis, digested wall	Penn state, never-dried	Quantitative DP	(s+G):i	1.5
Arabidopsis, WT intact	U Kentucky, rehydrated	Quantitative DP	(s+G):i	1.9
Arabidopsis, cesa1^{aegeus}/cesa3$^{ixr1\text{-}2}$	U Kentucky, rehydrated	Quantitative DP	(s+G):i	2.5

0.9 to 1.0, then the number of chains increases to 20–25, in good agreement with the current analysis. Indeed, the 2013 study pointed out that both the WAXS and SSNMR data can be fit with a 24-chain model if twinning is absent. The 18-chain model fits the s:i ratio of 1.8 only if at least 40% of the cellulose microfibrils twinned and all the chains on the twinning interface are converted to highly crystalline structures so that their C4 and C6 signals would resonate at 89 and 65 ppm. This crystallization process would require the establishment of many hydrogen bonds and likely conformational changes of the hydroxymethyl group. To our knowledge, these two requirements—a high degree of twinning in primary walls and the crystallization of surface chains upon twinning—have not been observed experimentally, thus cautioning against the interpretation of the 18-chain model.

The quantitative s:i ratios obtained from these SSNMR spectra place important constraints on the cellulose structural model. Our findings that some interior chains are more than one chain away from the nearest surface chains, together with the reduced s:i ratios of 1.2–1.5, both indicate that cellulose microfibrils in both dicot and grass primary walls should have sufficiently large dimensions to contain at least 24 chains.

Conclusions

Multidimensional ^{13}C SSNMR of ^{13}C-labelled plants is a powerful and versatile tool to elucidate the spatial proximities and structures of polysaccharides and proteins in near-native plant cell walls. Intermolecular cross peaks indicate that the primary wall of higher plants consists of a single cohesive network of polysaccharides, in which cellulose interacts with both hemicellulose and pectins on the nanometre scale. 2D ^{13}C-^{13}C correlation spectra and 1D quantitative ^{13}C NMR spectra of dicot and grass primary walls indicate that cellulose microfibrils contain at least 24 glucan chains. This size is sufficiently large for some of the interior chains to avoid direct contact with the surface chains, thus explaining the lack of intensity equilibration between the interior and surface cellulose ^{13}C signals at long spin diffusion mixing times. Future development of high-resolution SSNMR techniques

and the synergistic use of multiple techniques should lead to higher resolution structure of the cellulose microfibrils and their assemblies.

Supplementary data

Supplementary data are available at *JXB* online.

Fig. S1. Relationship of the chain number and s:i ratio of cellulose microfibrils.

Fig. S2. Cellulose microfibril models with various chain numbers and s:i ratios.

Acknowledgements

This work is supported by the Center for Lignocellulose Structure and Formation, an Energy Frontier Research Center funded by the US Department of Energy, Office of Science, Basic Energy Sciences under Award # DE-SC0001090. We thank Dr Paul White, Dr Yu Yang, and Jonathan Williams for helpful discussions.

References

Atalla RH, VanderHart DL. 1984. Native cellulose: a composite of two distinct crystalline forms. Science **223,** 283–285.

Atalla RH, VanderHart DL. 1999. The role of solid state ^{13}C NMR spectroscopy in studies of the nature of native celluloses. Solid State Nuclear Magnetic Resonance **15,** 1–19.

Bardet M, Emsley L, Vincendon M. 1997. Two-dimensional spin-exchange solid-state NMR studies of 13 C-enriched wood. Solid State Nuclear Magnetic Resonance **8,** 25–32.

Bax A, Freeman R, Kempsell SP. 1980. Natural abundance ^{13}C-^{13}C coupling observed via double-quantum coherence. Journal of the Amercian Chemical Society **102,** 4849–4851.

Bootten TJ, Harris PJ, Melton LD, Newman RH. 2004. Solid-state ^{13}C-NMR spectroscopy shows that the xyloglucans in the primary cell walls of mung bean (Vigna radiata L.) occur in different domains: a new model for xyloglucan-cellulose interactions in the cell wall. Journal of Experimental Botany **55,** 571–583.

Brabham C, Lei L, Gu Y, Stork J, Barrett M, DeBolt S. 2014. Indaziflam herbicidal action: a potent cellulose biosynthesis inhibitor. Plant Physiology **166,** 1177–1185.

Caffall KH, Mohnen D. 2009. The structure, function, and biosynthesis of plant cell wall pectic polysaccharides. Carbohydrate Research **344,** 1879–1900.

Carpita NC. 1983. Hemicellulosic polymers of cell walls of Zea coleoptiles. Plant Physiology **72,** 515–521.

Carpita NC, Gibeaut DM. 1993. Structural models of primary cell walls in flowering plants: consistency of molecular structure with the physical properties of the walls during growth. Plant Journal **3,** 1–30.

Carpita NC. 1996. Structure and biogenesis of the cell walls of grasses. Annual Review of Plant Physiology and Plant Molecular Biology **47,** 445–476.

Cavalier DM, Lerouxel O, Neumetzler L,*et al.* 2008. Disrupting Two Arabidopsis thaliana Xylosyltransferase Genes Results in Plants Deficient in Xyloglucan, a Major Primary Cell Wall Component. Plant Cell **20,** 1519–1537.

Cegelski L, O'Connor RD, Stueber D, Singh M, Poliks B, Schaefer J. 2010. Plant Cell-Wall Cross-Links by REDOR NMR Spectroscopy. Journal of the Amercian Chemical Society **132,** 16052–16057.

Cosgrove DJ. 2001. Wall structure and wall loosening. A look backwards and forwards. Plant Physiology **125,** 131–134.

Cosgrove DJ. 2005. Growth of the plant cell wall. Nature Reviews Molecular Cell Biology **6,** 850–861.

Cosgrove DJ. 2014. Re-constructing our models of cellulose and primary cell wall assembly. Current Opinion in Plant Biology **22C,** 122–131.

Dick-Perez M, Zhang YA, Hayes J, Salazar A, Zabotina OA, Hong M. 2011. Structure and interactions of plant cell wall polysaccharides by two- and three-dimensional magic-angle-spinning solid-state NMR. Biochemistry **50,** 989–1000.

Dick-Perez M, Wang T, Salazar A, Zabotina OA, Hong M. 2012. Multidimensional solid-state NMR studies of the structure and dynamics of pectic polysaccharides in uniformly ^{13}C-labeled Arabidopsis primary cell walls. Magnetic Resonance in Chemistry **50,** 539–550.

Dupree R, Simmons TJ, Mortimer JC, Patel D, Iuga D, Brown SP, Dupree P. 2015. Probing the Molecular Architecture of Arabidopsis thaliana Secondary Cell Walls Using Two- and Three-Dimensional ^{13}C Solid State Nuclear Magnetic Resonance Spectroscopy. Biochemistry **54,** 2335–2345.

Earl WL, VanderHart DL. 1981. Observations by High-Resolution Carbon- 13 Nuclear Magnetic Resonance of Cellulose I Related to Morphology and Crystal Structure. Macromolecules **14,** 570–574.

Endler A, Persson S. 2011. Cellulose Synthases and Synthesis in Arabidopsis. Mol. Plant **4,** 199–211.

Fernandes AN, Thomas LH, Altaner CM, Callow P, Forsyth VT, Apperley DC, Kennedy CJ, Jarvis MC. 2011. Nanostructure of cellulose microfibrils in spruce wood. Proceedings of the National Academy of Sciences of the United States of America **108,** E1195–E1203.

Fry SC. 1989. The structure and functions of xyloglucan. Journal of Experimental Botany **40,** 1–11.

Guerriero G, Fugelstad J, Bulone V. 2010. What do we really know about cellulose biosynthesis in higher plants? Journal of Integrative Plant Biology **52,** 161–175.

Harris DM, Corbin K, Wang T, *et al.* 2012. Cellulose microfibril crystallinity is reduced by mutating C-terminal transmembrane region residues $CESA1^{A903V}$ and $CESA3^{T942I}$ of cellulose synthase. Proceedings of the National Academy of Sciences of the United States of America **109,** 4098–4103.

Hediger S, Emsley L, Fischer M. 1999. Solid-state NMR characterization of hydration effects on polymer mobility in onion cell-wall material. Carbohydrate Research **322,** 102–112.

Hediger S, Lesage A, Emsley L. 2002. A new NMR method for the study of local mobility in solids and application to hydration of biopolymers in plant cell walls. Macromolecules **35,** 5078–5084.

Herth W. 1983. Arrays of plasma-membrane "rosettes" involved in cellulose microfibril formation of Spirogyra. Planta **159,** 347–356.

Hill JLJ, Hammudi MB, Tien M. 2014. The Arabidopsis cellulose synthase complex: a proposed hexamer of CESA trimers in an equimolar stoichiometry. Plant Cell **26,** 4834–4842.

Hohwy M, Rienstra CM, Jaroniec CP, Griffin RG. 1999. Fivefold symmetric homonuclear dipolar recoupling in rotating solids: Application to double quantum spectroscopy. Journal of Chemical Physics **110,** 7983–7992.

Horii F, Hirai A, Kitamaru R. 1987. CP/MAS C-13 NMR spectra of the crystalline components of native celluloses. Macromolecules **20,** 2117–2120.

Jarvis M. 2003. Chemistry: cellulose stacks up. Nature **426,** 611–612.

Jarvis MC. 1992. Self-assembly of plant cell walls. Plant Cell and Environment **15,** 1–5.

Johnson RL, Schmidt-Rohr K. 2014. Quantitative solid-state ^{13}C NMR with signal enhancement by multiple cross polarization. Journal of Magnetic Resonance **239,** 44–49.

Kennedy CJ, Cameron GJ, Sturcova A, Apperley DC, Altaner C, Wess TJ, Jarvis MC. 2007. Microfibril diameter in celery collenchyma cellulose: X-ray scattering and NMR evidence. Cellulose **14,** 235–246.

Kiemle SN, Zhang X, Esker AR, Toriz G, Gatenholm P, Cosgrove DJ. 2014. Role of (1,3)(1,4)-β-glucan in cell walls: interaction with cellulose. Biomacromolecules **15,** 1727–1736.

Komatsu T, Kikuchi J. 2013. Selective Signal Detection in Solid-State NMR Using Rotor-Synchronized Dipolar Dephasing for the Analysis of Hemicellulose in Lignocellulosic Biomass. Journal of Physical Chemistry Letters **4,** 2279–2283.

Kono H, Erata T, Takai M. 2003. Determination of the through-bond carbon-carbon and carbon-proton connectivities of the native celluloses in the solid state. Macromolecules **36,** 5131–5138.

Kono H, Numata Y. 2006. Structural investigation of cellulose I_α and I_β by 2D RFDR NMR spectroscopy: determination of sequence of magnetically inequivalent D-glucose units along cellulose chain. Cellulose **13,** 317–326.

Larsson PT, Hult EL, Wickholm K, Pettersson E, Iversen T. 1999. CP/MAS ^{13}C NMR spectroscopy applied to structure and interaction studies on cellulose I. Solid State Nuclear Magnetic Resonance **15,** 31–40.

Lesage A, Auger C, Caldarelli S, Emsley L. 1997. Determination of through-bond carbon-carbon connectivities in solid-state NMR using the INADEQUATE experiment. Journal of the Amercian Chemical Society **119,** 7867–7868.

Li S, Zhang Y, Hong M. 2010. 3D ^{13}C-^{13}C-^{13}C correlation NMR for de novo distance determination of solid proteins and application to a human alpha-defensin. Journal of Magnetic Resonance **202,** 203–210.

Matthews JF, Skopec CE, Mason PE, Zuccato P, Torget RW, Sugiyama J, Himmel ME, Brady JW. 2006. Computer simulation studies of microcrystalline cellulose I_β. Carbohydrate Research **341,** 138–152.

Mccann MC, Wells B, Roberts K. 1990. Direct visualization of cross-links in the primary plant cell wall. Journal of Cell Science **96,** 323–334.

Mccann MC, Roberts K, Wilson RH, Gidley MJ, Gibeaut DM, Kim JB, Carpita NC. 1995. Old and new ways to probe plant cell wall architecture. Canadian Journal of Botany **73,** S103–S113.

Newman RH, Ha MA, Melton LD. 1994. Solid-state ^{13}C NMR investigation of molecular ordering in the cellulose of apple cell walls. Journal of Agricultural and Food Chemistry **42,** 1402–1406.

Newman RH, Davies LM, Harris PJ. 1996. Solid-state ^{13}C nuclear magnetic resonance characterization of cellulose in the cell walls of Arabidopsis thaliana leaves. Plant Physiology **111,** 475–485

Newman RH, Hill SJ, Harris PJ. 2013. Wide-angle x-ray scattering and solid-state nuclear magnetic resonance data combined to test models for cellulose microfibrils in mung bean cell walls. Plant Physiology **163,** 1558–1567.

Nishiyama Y, Langan P, Chanzy H. 2002. Crystal structure and hydrogen-bonding system in cellulose I_β from synchrotron X-ray and neutron fiber diffraction. Journal of the Amercian Chemical Society **124,** 9074–9082.

Nishiyama Y, Kim UJ, Kim DY, Katsumata KS, May RP, Langan P. 2003a. Periodic disorder along ramie cellulose microfibrils. Biomacromolecules **4,** 1013–1017.

Nishiyama Y, Sugiyama J, Chanzy H, Langan P. 2003b. Crystal structure and hydrogen bonding system in cellulose Iα, from synchrotron X-ray and neutron fiber diffraction. Journal of the Amercian Chemical Society **125,** 14300–14306.

Park YB, Cosgrove DJ. 2012a. Changes in cell wall biomechanical properties in the xyloglucan-deficient xxt1/xxt2 mutant of arabidopsis. Plant Physiology **158,** 465–475.

Park YB, Cosgrove DJ. 2012b. A revised architecture of primary cell walls based on biomechanical changes induced by substrate-specific endoglucanases. Plant Physiology **158,** 1933–1943.

Park YB, Cosgrove DJ. 2015. Xyloglucan and its interactions with other components of the growing cell wall. Plant and Cell Physiology. **56,** 180–194.

Scheible WR, Eshed R, Richmond T, Delmer DP, Somerville C. 2001. Modifications of cellulose synthase confer resistance to isoxaben and thiazolidinone herbicides in Arabidopsis Ixr1 mutants. Proceedings of the National Academy of Sciences of the United States of America **98,** 10079–10084.

Sethaphong L, Haigler CH, Kubicki JD, Zimmer J, Bonetta D, DeBolt S, Yingling YG. 2013. Tertiary model of a plant cellulose synthase. Proceedings of the National Academy of Sciences of the United States of America **110,** 7512–7517.

Takegoshi K, Nakamura S, Terao T. 2001. ^{13}C-^{1}H dipolar-assisted rotational resonance in magic-angle spinning NMR. Chemical. Physics Letters **344,** 631–637.

Talbott LD, Ray PM. 1992. Molecular-size and separability features of Pea cell wall polysaccharides. Implications for models of primary wall structure. Plant Physiology **98,** 357–368.

Taylor NG. 2008. Cellulose biosynthesis and deposition in higher plants. New Phytologist **178,** 239–252.

Thomas LH, Forsyth VT, Sturcova A, Kennedy CJ, May RP, Altaner CM, Apperley DC, Wess TJ, Jarvis MC. 2013. Structure of cellulose microfibrils in primary cell walls from Collenchyma. Plant Physiology **161,** 465–476.

Vietor RJ, Newman RH, Ha MA, Apperley DC, Jarvis MC. 2002. Conformational features of crystal-surface cellulose from higher plants. Plant Journal **30,** 721–731.

Vogel J. 2008. Unique aspects of the grass cell wall. Current Opinion in Plant Biology **11,** 301–307.

Wang T, Zabotina O, Hong M. 2012. Pectin-cellulose interactions in the Arabidopsis primary cell wall from two-dimensional magic-angle-spinning solid-state nuclear magnetic resonance. Biochemistry **51,** 9846–9856.

Wang T, Park YB, Caporini MA, Rosay M, Zhong LH, Cosgrove DJ, Hong M. 2013. Sensitivity-enhanced solid-state NMR detection of expansin's target in plant cell walls. Proceedings of the National Academy of Sciences of the United States of America **110,** 16444–16449.

Wang T, Salazar A, Zabotina OA, Hong M. 2014. Structure and dynamics of Brachypodium primary cell wall polysaccharides from two-dimensional ^{13}C solid-state nuclear magnetic resonance spectroscopy. Biochemistry **53,** 2840–2854.

Wang T, Park YB, Cosgrove DJ, Hong M. 2015a. Cellulose-Pectin Spatial Contacts Are Inherent to Never-Dried Arabidopsis thaliana Primary Cell Walls: Evidence from Solid-State NMR. Plant Physiology **168,** 871–884.

Wang T, Williams JK, Schmidt-Rohr K, Hong M. 2015b. Relaxation-compensated difference spin diffusion NMR for detecting ^{13}C-^{13}C long-range correlations in proteins and polysaccharides. Journal of Biomolecular NMR **61,** 97–107.

White PB, Wang T, Park YB, Cosgrove DJ, Hong M. 2014. Water-polysaccharide interactions in the primary cell wall of Arabidopsis thaliana from polarization transfer solid-state NMR. Journal of the Amercian Chemical Society **136,** 10399–10409.

Woodward JR, Phillips DR, Fincher GB. 1988. Water-soluble (1->3,1->4)-β-D-glucans from Barley (Hordeum-Vulgare) Endosperm.IV. Comparison of 40°C and 65°C Soluble Fractions. Carbohydrate Polymer **8,** 85–97.

Zykwinska A, Thibault JF, Ralet MC. 2007. Organization of pectic arabinan and galactan side chains in association with cellulose microfibrils in primary cell walls and related models envisaged. Journal of Experimental Botany **58,** 1795–1802.